



# Structural, morphological, optical and magnetic properties of sprayed NiO thin films by perfume atomizer

S. Visweswaran<sup>1</sup> · R. Venkatachalapathy<sup>1</sup> · M. Haris<sup>2</sup> · R. Murugesan<sup>3</sup>

Received: 5 March 2020 / Accepted: 5 June 2020 / Published online: 15 June 2020  
© Springer-Verlag GmbH Germany, part of Springer Nature 2020

## Abstract

Nickel oxide (NiO) thin films were grown on glass substrates by a simplified spray pyrolysis technique using perfume atomizer at different substrate temperatures which is the novelty of this work. X-ray diffraction patterns reveal the cubic crystalline phase pure NiO film with preferential orientation along (2 0 0) plane. Thermal treatment of NiO thin films at 400 °C enables us to identify a suitable deposition temperature for obtaining good quality thin films. The average crystallite size calculated from Scherrer's formula is found to be 28 nm. The closely packed and spherical shaped grains obtained were confirmed from field emission-scanning electron microscope (FE-SEM). From FE-SEM analysis, the smooth nature of NiO thin films deposited at 400 °C enables it to use for solar cell applications, whereas the porous nature of NiO thin films deposited at 300 °C enables it to use for gas sensing applications. The mean square roughness increased with substrate temperature is confirmed from atomic force microscope analysis. The average transmittance of 75–85% demonstrates the compactness of the film except for the film N400, which is attributed to the defects. The energy band gap ( $E_g$ ) is found to be 2.93, 3.63, 3.72, and 3.67 eV, respectively, for NiO thin film deposited at substrate temperature 300 °C, 350 °C, 400 °C, and 450 °C. The Raman peak at 1573  $\text{cm}^{-1}$  corresponds to 2 M band antiferromagnetic state. The presence of defect states is identified from PL and EPR spectra.

**Keywords** NiO thin film · Various substrate temperature · Perfume atomizer · Spray pyrolysis · Structural and optical properties · Magnetic properties

## 1 Introduction

Nickel oxide belongs to periodic group X–VI, which is a p-type semiconducting material with band gap ranging from 3.6 to 4 eV [1–3]. The properties of NiO purely depend

on the ratio of nickel to oxygen atoms. NiO thin films can be prepared by several methods such as spray pyrolysis [4–7], sol-gel [8, 9], pulsed laser deposition [10, 11], electrochemical methods [12–15], DC/RF magnetron sputtering [16] and successive ionic layer adsorption and reaction (SILAR) [17–19]. Due to its small size, large surface area, high surface energies [20] and various morphologies like nano-sheets [21], nano-wires [22], nano-fibres [23], cactus like nano-structure [24], hemisphere [25], nano-flowers [26] with size ranging from several nanometers to micrometers, NiO thin films were used in variety of technology-based applications such as gas sensors [27], electrochromic devices [28], dye sensitized solar cells [29], resistive switching [30], catalysts [31], batteries [32], water splitting application [33], energy storage [34], superparamagnetic devices [35], transparent electrode and opto-electronic devices [36]. Uchida et al. reported the phase pure single crystalline NiO thin film by metal organic vapor phase epitaxy technique [37]. Nano-sized porous NiO thin film shows high photocatalytic activity of commercially available dyes such as

✉ S. Visweswaran  
visudharan@gmail.com

R. Venkatachalapathy  
rvcasmb@gmail.com

M. Haris  
harismuthiah@gmail.com

R. Murugesan  
murugesm629@gmail.com

<sup>1</sup> Department of Physics, Annamalai University,  
Chidambaram Annamalai Nagar 608 002, India

<sup>2</sup> Department of Applied Physics, Karunya Institute  
of Technology and Sciences, Coimbatore 641 114, India

<sup>3</sup> Department of Physics, Thiru Kolanjiappar Government Arts  
College, Vridhachalam 606 001, India

methyl orange, indicating the NiO can be used for pollutant cleanup [38]. Navale et al. investigated the electrochemical supercapacitor behavior of amorphous NiO thin film by electrodeposition at various time intervals. The supercapacitor performances were within the potential range of  $-1.2$  to  $+1.2$  V [39]. Shang et al. [40] explored NiO with rose like nanostructure exhibits high photocatalytic activity. More recently, the ferromagnetic (FM) phenomenon of NiO-based nanoparticles and thin film made it suitable for spintronic devices [41, 42]. The NiO was chosen as alternative anode material for lithium ion battery with a high capacitance value of 718 mAh/g which was reported by Huang et al. [43]. Kate et al. [44] reported the effect of substrate temperature on the spray deposited NiO thin films. The preferred orientation (1 1 1) remains constant for the films at different temperatures and also morphology of the thin film. The substrate temperature strongly affects the thickness and energy gap of the NiO film which were explained by Bakry et al. [45]. This paper reports on the preparation of phase pure NiO thin film by custom made spray pyrolysis technique using perfume atomizer, and their structural, morphological, optical properties were studied. The novelty of this research work is employing a simple and efficient ambient pressure perfume atomizer as an alternative to conventional spray pyrolysis instrument. This also results in obtaining NiO thin films with appreciable properties by varying the substrate temperature during spray deposition. Thermal treatment of NiO thin films at 400 °C enables us to identify a suitable deposition temperature for obtaining good quality thin films. From FE-SEM analysis, the smooth nature of NiO thin films deposited at 400 °C enables it to use for solar cell applications, whereas the porous nature of NiO thin films deposited at 300 °C enables it to use for gas sensing applications.

## 2 Experimental

To synthesize NiO thin film, nickel acetate anhydrate ( $\text{Ni}(\text{CH}_3\text{COO})_2 \cdot x\text{H}_2\text{O}$ ) 99% purchased from Alfa Aesar was used without further purification. Ethanol (AR grade) was used as a solvent. Blue star (Mumbai) and micro-glass slides ( $75 \times 25$  mm) (PIC - 1) were used as substrate for film deposition. The glass substrate was washed with soap solution and is degreased using hydrochloric acid (AR grade, Merck) and acetone (AR grade, Merck), finally rinsed in deionized water and dried for 30 min. Then the glass substrate was placed on the heating plate at the desired temperature prior to deposition [46, 47]. A 0.1 M of nickel acetate precursor was diluted in the mixture of double distilled water and ethanol in 2:1 ratio. The mixture was dispersed ultrasonically (stainless steel sonicator bath, Ikon Industries, Mumbai) for about 20 min in a water bath maintained at 60 °C, resulting in a homogeneous and transparent solution. This final

solution is sprayed on to the preheated substrate maintained at 300 °C, 350 °C, 400 °C, and 450 °C, respectively, using the perfume atomizer for film deposition. The sketch of simplified perfume spray pyrolysis setup is shown in Fig. 1. The as-deposited films were then annealed at 450 °C for 1 h and were characterized by X-ray diffraction, field emission-scanning electron microscopy, atomic force microscope, ultraviolet–visible spectrophotometer, photoluminescence analyzer, Raman analyzer and electron paramagnetic resonance spectroscopy.

## 3 Results and discussion

### 3.1 X-ray diffraction analysis

The structure and phase of the NiO thin film were analyzed by PANalytical/Xpert3 powder XRD diffraction instrument. The structural characterization of NiO film deposited at temperatures 300 °C, 350 °C, 400 °C, and 450 °C is displayed in Fig. 2. The XRD patterns reveal crystalline, pure phase NiO film with cubic structure. The diffraction peaks at 37.20°, 43.23°, 62.81° and 75.72° correspond to (1 1 1), (2 0 0) and (3 1 1) crystallographic planes, respectively.

No other impurities are observed within the detection limits. The obtained diffraction peaks are in good agreement with the JCPDS No. 89 - 7130. It shows the preferential orientation along (2 0 0) plane, indicating that the NiO film has favorable growth along (2 0 0) direction. All samples have the same structural pattern where only the intensity varies. This could be a good indicative of the crystallinity of the film [17]. The intensity of diffraction peaks increased with substrate temperature up to 400 °C

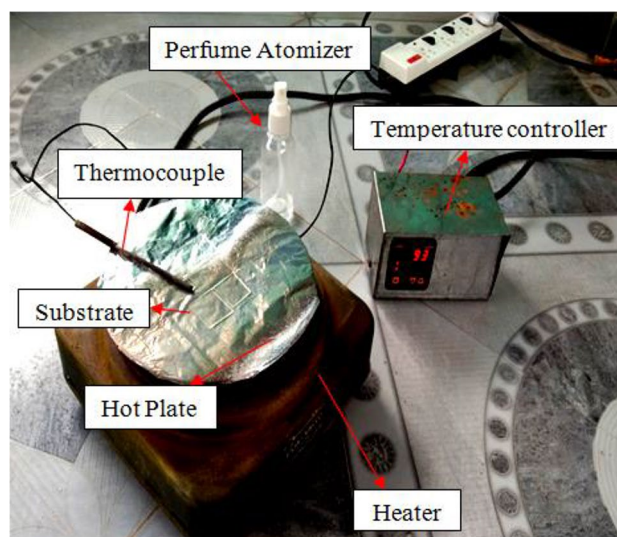
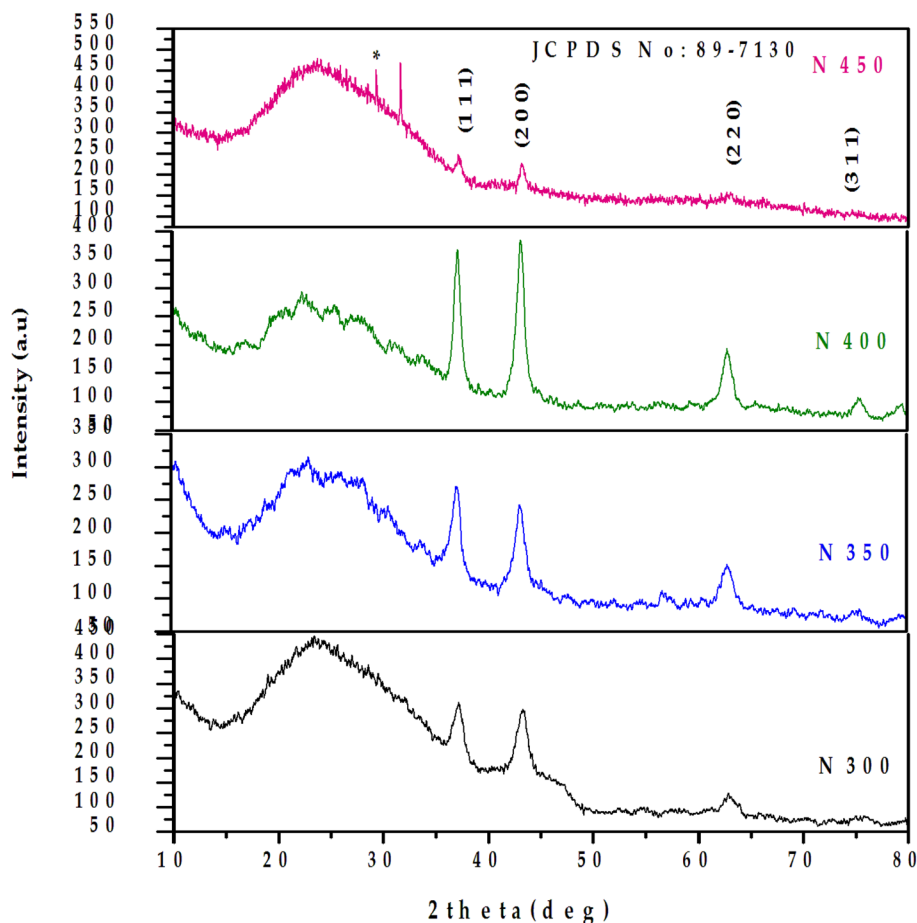


Fig. 1 Schematic of simplified perfume spray pyrolysis setup

**Fig. 2** XRD patterns of NiO film deposited at various substrate temperatures



is due to the enlargement and densification of grains. And at 450 °C, the intensity of diffraction peak decreases. The decrease in intensity of XRD at 450 °C might be due to homogeneous reaction and incomplete thermal decomposition; as a result, it induces atomic level strain leading to some random and irregular grains as seen from FE-SEM morphologies [48, 49]. The significant decrease in the intensity of diffraction peaks at higher temperatures is also attributed to the deterioration of crystallinity and the strain produced [50]. The broad hump and peak around 29° (marked as \*) in the XRD pattern of N450 denote the amorphous state of the substrate used [51]. Additionally, Ni<sub>2</sub>O<sub>3</sub> hexagonal phase along (0 0 2) plane at 2θ (31.66°) (JCPDS Card Number 14-0481) is observed for the film deposited at 450 °C [52]. Najafi et al. reported the presence of Ni<sub>2</sub>O<sub>3</sub> phase for Cu-doped NiO thin film by spray pyrolysis [53]. As the temperature is increased, the density of nucleation centers decreases. As a consequence, a small number of nucleation centers start to grow resulting in larger grains [54]. The similar trend in spray deposited NiO thin film has been revealed by Krunks et al. [55], as the temperature goes high, the thickness of the film is lowered which is a typical nature of spray process wherein

the spray droplets drive away from the reaction zone and only few precursor reaches the substrate.

The parameters, such as crystallite size ( $D$ ), microstrain ( $\epsilon$ ), dislocation density ( $\delta$ ), d-spacing, unit cell volume, are tabulated in Table 1.

The crystallite size ( $D$ ) is calculated from the diffraction peak using Scherrer's relation,

$$D = \kappa \lambda / \beta \cos \theta \text{ (nm)}$$

' $D$ ' is the crystallite size (nm), ' $\kappa$ ' is the shape factor (0.9), ' $\lambda$ ' is the x-ray wavelength (1.540 Å), ' $\beta$ ' the full width and half maxima (radian), and ' $\theta$ ' is the Bragg's angle (degree).

The microstrain ( $\epsilon$ ) was calculated using the formula,

$$\text{Microstrain}(\epsilon) = \frac{(a - a_0)}{a_0} \times 100\%$$

In general, if  $\epsilon > 0$ , it represents tensile strain and if  $\epsilon < 0$ , it leads to compressive strain, respectively. For spray deposited NiO thin films, the strain,  $\epsilon > 0$ , clearly states that the NiO thin film exhibits tensile strain as the result of excess oxygen [56].

**Table 1** Crystallite size ( $D$ ), microstrain ( $\epsilon$ ), dislocation density ( $\delta$ ), d-spacing, lattice constant and unit cell volume of NiO thin film

Substrate temperature ( $T_s$ ) (°C)	Hkl plane	$2\theta$ (deg)	FWHM (radian)	d-spacing (Å)	Crystallite size ( $D$ ) (nm)	Micro-strain ( $\epsilon$ ) (%)	Dislocation Density ( $\delta$ ) (lines/m <sup>2</sup> )	Lattice constant (a) Å	Volume of unit cell (a <sup>3</sup> ) (Å <sup>3</sup> )
300	111	37.11	0.8725	2.420	10.03	0.316	0.0099	4.181	73.087
	200	43.23	1.2609	2.090	7.08		0.0199		
	220	62.86	0.7897	1.477	12.31		0.0065		
350	111	37.15	1.1338	2.417	7.72	0.388	0.0167	4.184	73.244
	200	43.22	1.2947	2.091	6.89		0.0210		
	220	62.67	2.1292	1.481	4.56		0.0480		
400	111	37.20	0.3420	2.414	25.6	0.172	0.0015	4.175	73.772
	200	43.23	0.9865	2.091	9.05		0.0122		
	220	62.81	1.7084	1.478	5.68		0.0309		
	311	75.72	0.8432	1.260	12.45		0.0064		
450	111	37.23	0.3456	2.412	25.34	0.292	0.0015	4.180	73.034
	200	43.26	0.0973	2.090	91.74		0.0001		
	220	62.98	9.7284	1.474	1		1		

The dislocation density ( $\delta$ ) is determined using

$$\delta = 1/D^2 (\text{lines/m}^2)$$

The lattice constant ( $a$ ) is calculated using

$$a = \frac{\lambda}{2 \sin \theta} \sqrt{(h^2 + k^2 + l^2)} \text{ \AA}$$

### 3.2 Field emission-scanning electron microscopy analysis

The surface morphology was observed by FE-SEM with EDX analyzer by Zeiss (SIGMA), Bruker instrument. The morphology of NiO film deposited on the glass substrate at substrate temperature 300 °C, 350 °C, 400 °C and 450 °C was analyzed and is displayed in Fig. 3a–d, respectively.

The SEM morphologies of almost all films appear to have spherical grains throughout their entire surface. The surface morphology of the deposited NiO film appears quasismooth, and uniform surfaces with closely packed spherical grains indicate the quality nature of the obtained film. The nanocrystalline grains with pores on the surface of the film are shown in Fig. 3a. The porous structure of the film entails for larger surface area increases the gas sensing property of sensors [57]. A smooth film with surface morphology such as those from Fig. 3b–c is the basic requirement for device applications such as electronics and optoelectronic devices. Similar morphology is observed for NiO thin films which are reported [11, 15]. Also the rice husk shaped grains are seen in Fig. 3d. A significant change in the morphologies is identified for the film as substrate temperature increases. At 450 °C, the film beneath the particles appears smooth and

dense [5, 55, 58]. Ukoba et al. studied the morphologies of NiO thin film at different precursor concentrations by spray pyrolysis showing husk-shaped grain [59]. The EDX spectrum of NiO thin film as the function of substrate temperature is shown in Fig. 4 and clearly reveals the oxygen-rich NiO film, and their corresponding atomic and weight % are presented in Table 2.

Besides the prominent peaks of Ni and O, the peak of Si is also observed, which is from the glass substrate, as the electron penetration depth is higher than film thickness [60]. The atomic ratio of oxygen to nickel in NiO film was reported by Hajakbari deposited by DC sputtering technique [66]. The nonstoichiometric NiO creates excess oxygen at Ni<sup>2+</sup> sites leading to more Ni vacancy [61].

### 3.3 Atomic Force Microscopy Analysis

The surface topography of NiO film was analyzed using AGILENT 5500 Atomic Force Microscope in contact mode. Figure 5a, c, e, g and b, d, f, h represents the 2D and their corresponding 3D AFM images of the NiO film at substrate temperatures 300 °C, 350 °C, 400 °C and 450 °C, respectively.

In general, the bright region of the image represents high peaks and deep valleys on the surface and the dark area is contradictory to the bright one [62]. An exceptionally rough surface with various pores was observed for NiO thin film deposited at 300 °C. A further decrease in porosity nature has been observed for the film deposited at 350 °C. Further the porosity has been diminished upon the expansion in substrate temperature up to 450 °C. Similar trend has been seen in SEM photographs. An increment in deposition temperature to 450 °C prompts film crackness and agglomeration

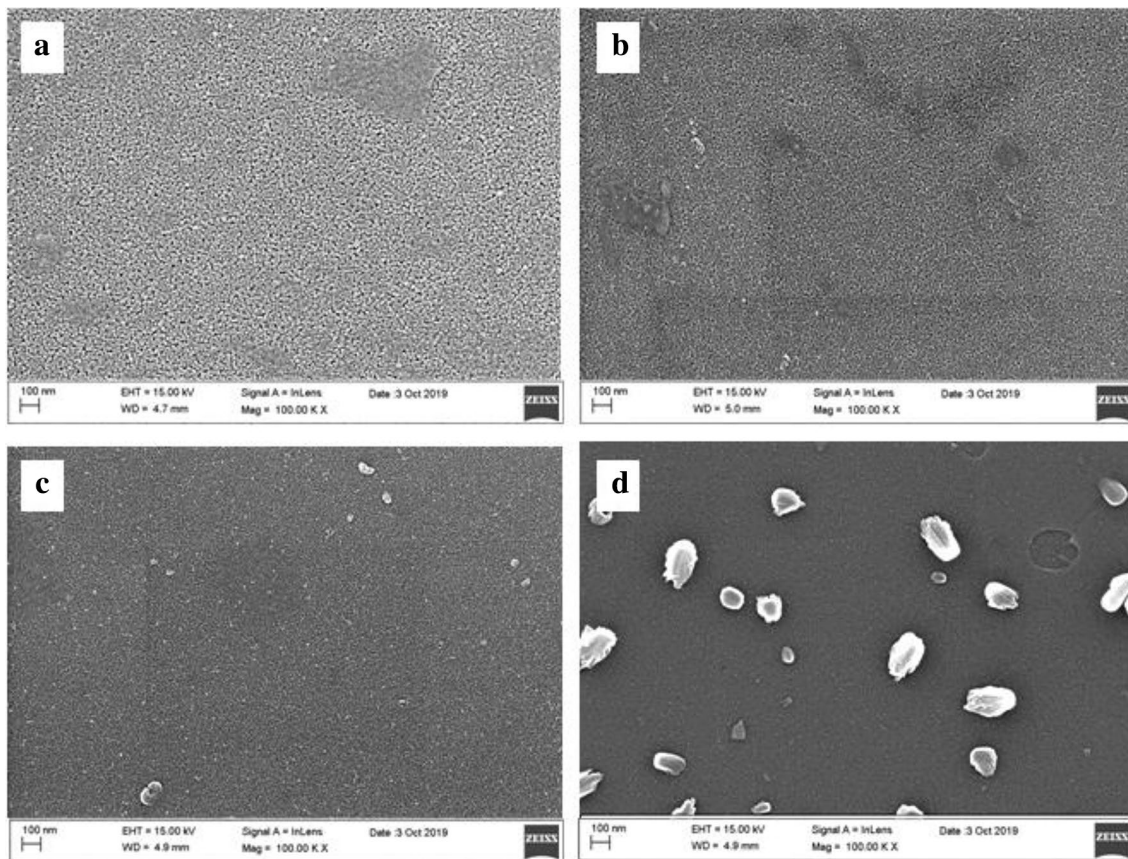


**Fig. 3** SEM micrograph of sprayed NiO thin film at substrate temperatures **a** 300 °C, **b** 350 °C, **c** 400 °C, and **d** 450 °C

of particles seen through SEM just as AFM. The estimated values of root-mean-square roughness ( $R_q$ ), height ( $R_a$ ), skewness ( $R_{sk}$ ), and kurtosis ( $R_{ka}$ ) for all the samples are given in Table 3.

### 3.4 Optical analysis

#### 3.4.1 Ultra violet–visible analysis

The UV–Vis absorbance and transmittance spectra of NiO thin film deposited at substrate temperatures 300 °C, 350 °C, 400 °C, and 450 °C were recorded in wavelength range 190–1100 using THERMOFISHER Evaluation 220 instrument which are displayed in Fig. 6. The NiO thin film deposited on the glass substrate at different temperatures is black, which is due to non-stoichiometry of the deposited film [63]. Normally the nickel oxide appears pale green. The nonstoichiometry of NiO thin film appears black. This may be due to the presence of nickel vacancy and interstitial oxygen or mixed valence  $\text{Ni}^{2+}/\text{Ni}^{3+}$  [57, 64]. Thus, the non-stoichiometric NiO contains  $\text{Ni}^{2+}$  vacancies, and this  $\text{Ni}^{2+}$  is oxidized to  $\text{Ni}^{3+}$  ions to keep charge neutral. [65, 66].

The absorbance of the thin film in Fig. 6 tends to decrease at a higher wavelength. This absorbance behavior is quite different for the thin film deposited at 400 °C. The same is the case with the transmittance also. It is noticed from the absorbance spectra that the maximum absorbance of all the samples can be found in the UV region around 300 nm wavelength.

Figure 7 displays the transmittance spectra of NiO thin film. The transmittance of NiO thin film decreased with substrate temperature is observed [67]. The transmittance of above 70% is noticed for all the films except for the film deposited at 400 °C. The transmittance of the thin film is related to defects such as the oxygen vacancy, impurities, and surface roughness of the deposited film [68]. Also, the sudden decrease in transmittance at substrate temperature 400 °C may be connected to the film's thickness. The absorption edge near 310 nm is observed for all the film which led the luminescence efficiency [69]. Here, the transmittance spectra show two regions, one at a wavelength above 400 nm, the transmission ranges from 75 to 88% is due to the compactness of the samples. Secondly, for the wavelength below 400 nm, all samples exhibit fundamental absorption due to the shift of electrons from

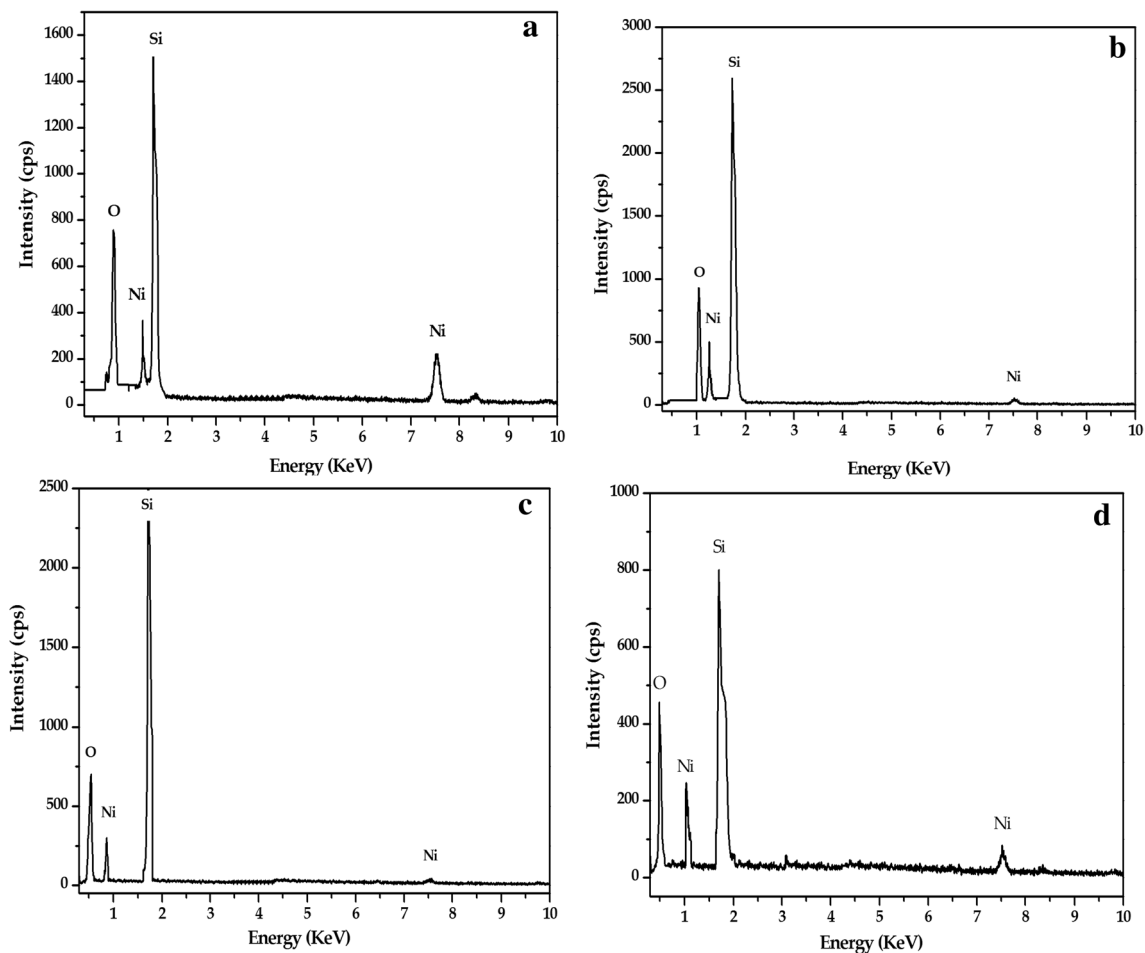


**Fig. 4** EDS spectra of spray deposited NiO thin films **a** 300 °C, **b** 350 °C, **c** 400 °C, and **d** 450 °C

**Table 2** Atomic and weight % of NiO thin film

Substrate temperature $T_s$ (°C)	Weight %			Atomic %		
	Ni	O	Si	Ni	O	Si
300	27.29	58.55	14.16	19.70	71.33	8.97
350	28.61	59.33	12.06	20.24	70.19	9.57
400	29.60	58.98	11.42	21.01	69.45	9.54
450	29.35	58.89	11.76	20.77	69.84	9.39

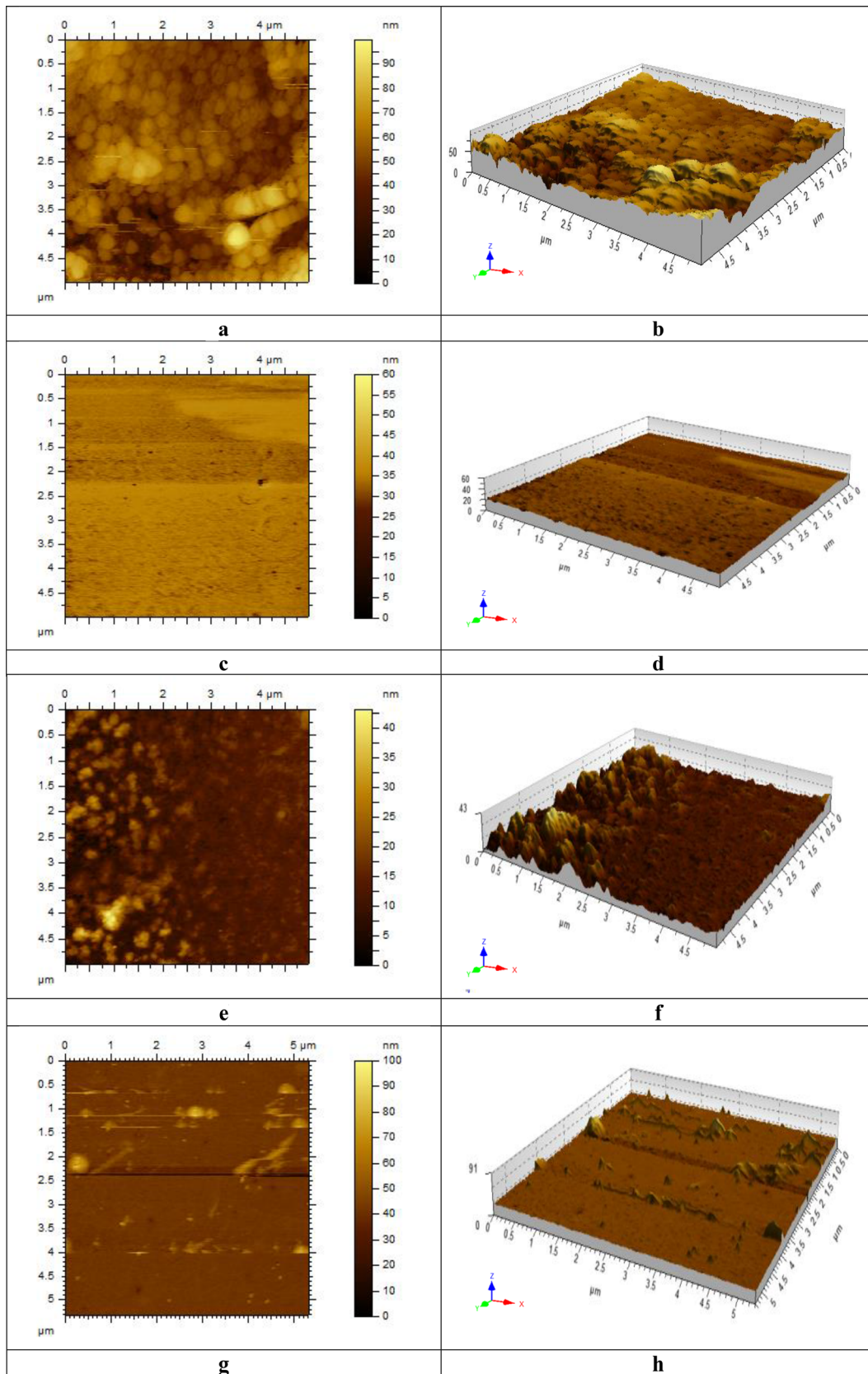
the valence band to conduction band [70]. Further, the transmittance spectra of the deposited thin film show no interference sign, which is due to the absence of multiple reflections inside the substrate. This is related to the thickness of the deposited film [71]. The average transmittance of the N400 sample is 36% which is in decreasing trend compared to the other thin film samples. This is attributed to more defects in the thin film. Such behavior is related with a higher conductivity of NiO thin films [72].

The optical energy band gap of NiO thin films is derived from absorbance spectra using well-known Tauc relation.

$$(\alpha h\nu)^{\left(\frac{1}{n}\right)} = A(h\nu - E_g)$$

Here, ' $\alpha$ ' is the absorption coefficient, ' $h\nu$ ' is the incident photon energy, ' $A$ ' is a constant, and ' $n$ ' is the exponent value which depends on the type of electronic transition such as direct or indirect. In our case, ' $n$ ' takes the value  $\frac{1}{2}$  and has a direct transition [70]. The optical band gap versus photon energy (eV) is shown in Fig. 8.

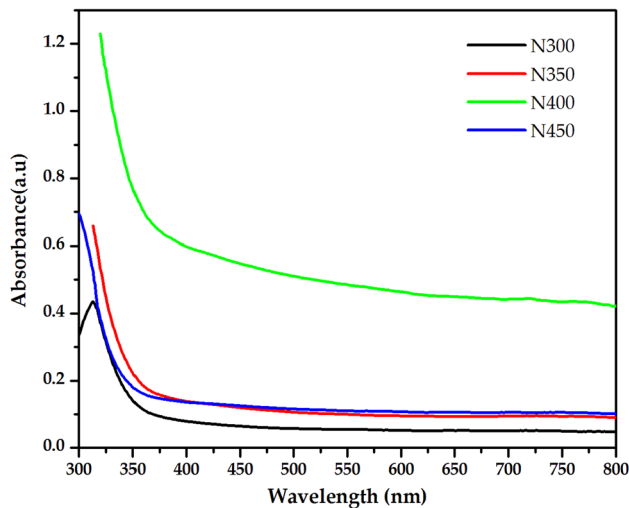
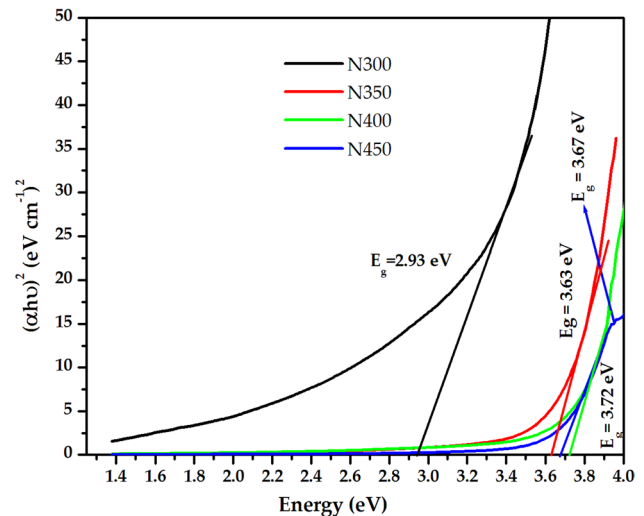
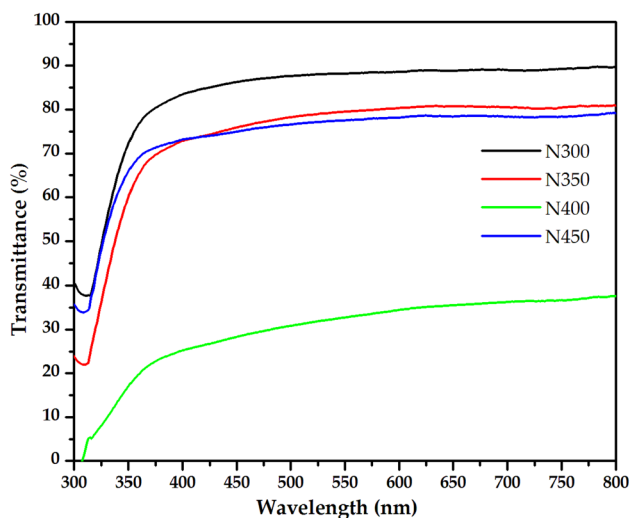
The spectral shape for NiO film at 450 °C is similar to the spectral shape of NiO thin film reported [70, 73, 78].



**Fig. 5** a–h 2D and 3D AFM images of NiO thin film deposited at different substrate temperature

**Table 3** Estimated values of root mean square roughness ( $R_q$ ), height ( $R_a$ ), skewness ( $R_{sk}$ ) and kurtosis ( $R_{ku}$ )

Substrate Temperature (°C)	$R_q$ nm	$R_a$ nm	$\frac{R_q}{R_a}$	$R_{sk}$	$R_{ku}$	$R_z$ nm
300	311.1	294.6	1.056	-0.294	-1.447	153
350	314.3	306.6	1.025	-0.129	-1.618	468
400	316.3	307	1.030	-0.164	-1.634	107
450	301.3	292.2	1.031	-0.192	-1.547	125

**Fig. 6** Absorbance spectrum of NiO Film**Fig. 8** The variation of  $(\alpha h\nu)^2$  versus Photon energy (eV) of NiO film**Fig. 7** Transmittance spectra of NiO film deposited at different substrate temperature

The values of the optical band gap are 2.93, 3.63, 3.72, and 3.67 eV, respectively, for the film deposited at various substrate temperatures and the value is comparable with the previous report [38].

### 3.5 Photoluminescence analysis

The room-temperature photoluminescence (PL) measurements were taken using Varian Cary Eclipse photoluminescence analyzer. Figure 9 represents the room-temperature PL spectra of NiO film at excitation wavelength of 310 nm. The PL spectra of NiO film exhibit one strong and several broad emission peaks in UV and visible regions, respectively. The strong UV emission at 360 nm observed for all samples is related to the NBE emission of NiO. This is due to the direct recombination of excitons through an exciton–exciton scattering. This could be assigned to the electronic transition between  $Ni^{2+}$  and  $O^{2-}$  ions [74].

Several broad emission peaks from 400 to 600 nm are due to deep level emission (DLE) [75]. The emission peak in the visible region is ascribed to the near band to band transition and defects such as oxygen vacancies, oxygen interstitials, nickel vacancies [76]. Also the absorption peak below 4 eV is dependent on interionic  $3d^8 - 3d^8$  transitions of  $Ni^{2+}$  which were reported by Adler and Feinleib [77]. The peaks in the violet region are due to  $p-d$  charge transfer, and the peaks around 504–537 nm are due to  $d-d$  transition of NiO.



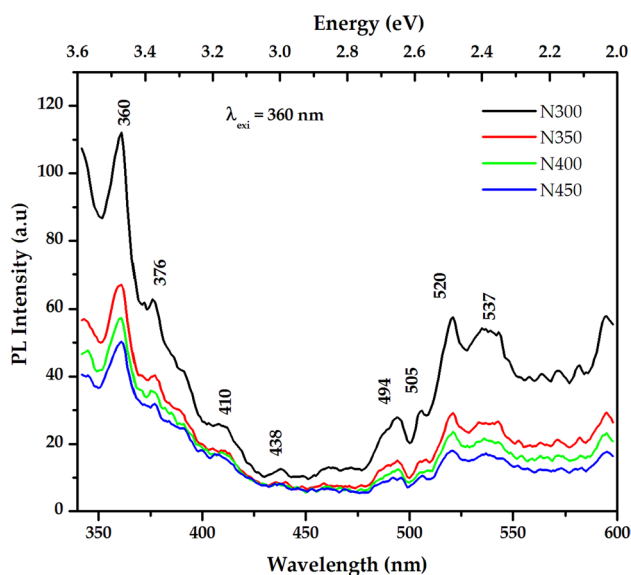


Fig. 9 Room-temperature PL spectra of NiO film

### 3.6 Raman analysis

The room-temperature Raman spectra of NiO film deposited on the glass substrate at various substrate temperatures are recorded through micro-Raman spectrometer SEKI, Japan. Figure 10 presents the superposed Raman spectra of NiO thin films, where the effect of Si/SiO<sub>2</sub> is subtracted and also compared with the previous literature [78].

There are four dominant Raman peaks noticed for all the film and an additional Raman peak at 1573 cm<sup>-1</sup> is observed for the film deposited at 450 °C along with a shift of around 10 cm<sup>-1</sup>. The origin of Raman shift is due to defects such

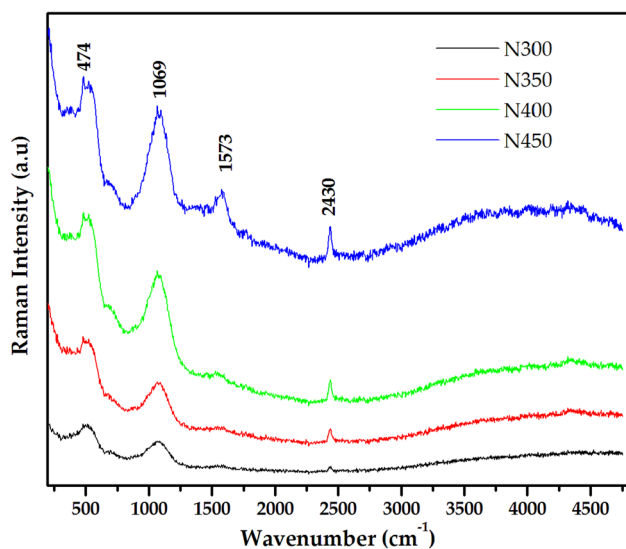


Fig. 10 Room-temperature Raman spectra of NiO film

as vacancy, substitution, interstitials, or dislocation. The Raman peak at 474 cm<sup>-1</sup> and 1069 cm<sup>-1</sup> is due to the Ni–O stretching mode [79]. From the Raman spectra, the peak at 474 and 696 cm<sup>-1</sup> is assigned to first-order transverse optical (TO) and (LO) phonon modes of NiO. The peak at 1069 cm<sup>-1</sup> is assigned to two phonon modes (2LO), as well as two magnon excitations at 1573 cm<sup>-1</sup> [79]. The Raman peak at 1573 cm<sup>-1</sup> corresponds to 2 M band that is associated with Ni<sup>2+</sup>–O<sup>2-</sup>–Ni<sup>2+</sup> superexchange interaction. It indicates the particle exists in the antiferromagnetic state at room temperature [80]. The Raman band at ~2430 cm<sup>-1</sup> corresponds to 4 M scattering. Similar 2 M Raman band is reported by N. Mironova-Ulmane et al. [81].

### 3.7 Electron paramagnetic resonance analysis

The EPR technique is used for identifying the material with unpaired electron and defects. The room-temperature EPR measurements for NiO film were recorded using EPR spectrometer Bruker EMX Plus operating at X-band (9.8 GHz) frequency with magnetic field modulation of 100 kHz and are displayed in Fig. 11. The EPR measurement is taken for the NiO thin film deposited at substrate temperature 350 °C and 400 °C. The change in EPR intensity and the line width is noticed from the spectrum. The observed EPR spectra arise as the results of paramagnetic sites or intrinsic defects in the sample. The presence of more than one paramagnetic or defects is identified from the spectra. The intensity of the EPR signal is very high for the sample N350 compared to the N400. The Ni<sup>2+</sup> ions have 3d<sup>8</sup> electronic configuration, whereas those Ni<sup>3+</sup> have 3d<sup>7</sup> configuration, both species being EPR active due to the existence of the uncoupled electrons. The unpaired electrons suggest the paramagnetic characteristics of NiO thin

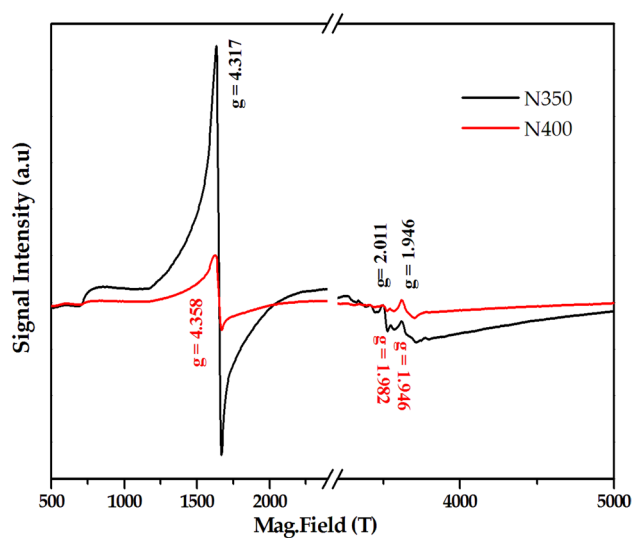


Fig. 11 Room-temperature EPR spectra of NiO film

film. The EPR sign designates the mixed valence of Ni<sup>2+</sup> and Ni<sup>3+</sup> ions. The presence of a broad line located nearly at the lower field is a typical nature for FMR (ferro magnetic resonance) [82]. As is seen, the particle size of NiO thin film is less than 100 nm, led to the transition of antiferromagnetic to paramagnetic state [83].

The Landé *g*-factor value is calculated using the equation.

$$g = h\nu/\mu_B B$$

where '*h*' is the Planck's constant, '*ν*' is microwave frequency, '*μ<sub>B</sub>*' is the Bohr magneton and '*B*' is the magnetic field (mT).

The calculated EPR *g* values for sample N350 films are 4.317, 2.011, and 1.946 and that of sample N400 are 4.358, 1.982, and 1.946. The *g* value 2.011 is associated with a coupled pair of Ni<sup>2+</sup>-O-Ni<sup>2+</sup> ions and the enhanced intensity and high *g* values represent the amount of Ni<sup>3+</sup> ions [84–86]. So, this EPR signal arises due to the intrinsic defect such as Ni vacancies and oxygen deficiency [87].

## 4 Conclusion

NiO thin films were deposited on glass substrates with different substrate temperatures by spray pyrolysis using perfume atomizer. The influence of substrate temperature on the structural, morphological, and topography of the films was studied from XRD, FESEM, and AFM analysis. The cubic crystalline NiO films with preferred orientation along (2 0 0) plane are obtained. The good quality of the film obtained at 400 °C is confirmed from XRD. The FESEM images exhibit nanocrystalline grains with uniform and smooth surface as the function of substrate temperature and the film at 450 °C shows rice husk shaped morphology. The AFM images shown rough surface with pores of NiO thin film deposited at 300 °C which should be the best suited for gas sensor applications. The oxygen-rich nonstoichiometric NiO is confirmed from EDS results. The mixed valence of Ni<sup>2+</sup>/Ni<sup>3+</sup> ions in NiO is responsible for the coloration of NiO film. The transmittance of above 70% is achieved from UV–Vis analysis seems inspiring for optoelectronics usages. The calculated direct band gap values for the NiO thin film at different substrate temperatures are 2.93, 3.63, 3.72 and 3.67 eV, respectively. The PL emission in the visible region is related to defects arising from oxygen vacancy. The antiferromagnetic nature of NiO films is identified from Raman spectra. The presence of defect states such as Ni vacancies and oxygen deficiency is noticed from EPR.

## References

- H. Yang, Q. Tao, X. Zhang, A. Tang, J. Ouyang, Solid-state synthesis and electrochemical property of SnO<sub>2</sub>/NiO nanomaterials. *J. Alloy. Compd.* **459**, 98–102 (2008)
- A.A. Al-Ghamdi, M. Sh Abdel-wahab, A.A. Farghali, P.M.Z. Hasan, Structural, optical and photo-catalytic activity of nanocrystalline NiO thin films. *Mater. Res. Bull.* **75**, 71–77 (2016)
- R. Kumar, C. Baratto, G. Faglia, G. Sberveglieri, E. Bontempi, L. Borgese, Tailoring the textured surface of porous nanostructured NiO thin films for the detection of pollutant gases. *Thin Solid Films* **583**, 233–238 (2015)
- R. Murugesan, S. Sivakumar, K. Karthik, P. Anandan, M. Haris, Structural, optical and magnetic behaviors of Fe/Mn-doped and co-doped CdS thin films prepared by spray pyrolysis method. *Appl. Phys. A* **125**, 281 (2019)
- J. Mathiyani, D. Sivalingam, J.B. Gopalakrishnan, J.B.B. Rayappan, Spray coated nanostructured NiO thin films for ethanol sensing. *J. Appl. Sci.* **12**, 1686–1690 (2012)
- Muhammad Awais, Denis P. Dowling, Franco Decker, Danilo Dini, Electrochemical characterization of nanoporous nickel oxide thin films spray-deposited onto indium-doped tin oxide for solar conversion scopes. *Adv. Condens. Matter Phys.* **2**, 1–18 (2015)
- S.L. Che, K. Takada, K. Takashima, O. Sakurai, K. Shinozaki, N. Mizutani, Preparation of dense spherical Ni particles and hollow NiO particles by spray pyrolysis. *J. Mater. Sci.* **34**, 1313–1318 (1999)
- A.M. Soleimanpour, Y. Hou, A.H. Jayatissa, Evolution of hydrogen gas sensing properties of sol-gel derived nickel oxide thin film. *Sens. Actuators B* **182**, 125–133 (2013)
- Said Benramache, Mansour Aouassa, Preparation and characterization of p-type semiconducting NiO thin films deposited by sol-gel technique. *J. Chem. Mater. Res.* **5**, 119–122 (2016)
- H.Q. Dai, Y.N. Zhou, Q. Sun, F. Lu, Z.W. Fu, Enhanced electrochemical properties of NiO/NiS nanocomposite thin film. *Electrochim. Acta* **76**, 145–151 (2012)
- I. Fasaki, A. Giannoudakos, M. Stamataki, M. Kompitsas, E. György, I.N. Mihailescu, F. Roubani-Kalantzopoulou, A. Lagoyannis, S. Harissopoulos, Nickel oxide thin films synthesized by reactive pulsed laser deposition: characterization and application to hydrogen sensing. *Appl. Phys. A* **91**, 487–492 (2008)
- J.S. Kang, J. Kim, J.S. Kim, K. Nam, H. Jo, Y.J. Son, J. Kang, J. Jeong, H. Choe, T.-H. Kwon, Y.-E. Sung, electrochemically synthesized mesoscopic nickel oxide films as photocathodes for dye-sensitized solar cells. *ACS Appl. Energy Mater.* **1**, 4178–4185 (2018)
- M.P. Browne, H. Nolan, N.C. Berner, G.S. Duesberg, P.E. Colavita, M.E.G. Lyons, Electrochromic nickel oxide films for smart window applications. *Int. J. Electrochem. Sci.* **11**, 6636–6647 (2016)
- M.-S. Wu, Y.-A. Huang, C.-H. Yang, J.-J. Jow, Electrodeposition of nanoporous nickel oxide film for electrochemical capacitors. *Int. J. Hydrogen Energy* **32**, 4153–4159 (2007)
- Vijay V. Kondalkar, Pallavi B. Patil, Rahul M. Mane, Pramod S. Patil, Sipra Choudhury, Popatrao N. Bhosal, Electrochromic performance of nickel oxide thin film: synthesis via electrodeposition technique. *Macromol. Symp.* **361**, 47–50 (2016)
- M. Guzewicz, P. Klata, J. Grochowski, K. Golaszewska, E. Kaminska, J.Z. Domagala, B.A. Witkowski, M. Kandyła, Ch. Chatzimanolis, M. Kompitsas, A. Piotrowska, Hydrogen sensing properties of thin NiO films deposited by RF sputtering. *Procedia Eng.* **47**, 746–749 (2012)
- Y. Akaltun, T. Çayır, Fabrication and characterization of NiO thin films prepared by SILAR Method. *J. Alloys Compd.* **625**, 144–148 (2015)
- Julien Bachmann, Andriy Zolotaryov, Ole Albrecht, Silvana Goetze, Andreas Berger, Dietrich Hesse, Dmitri Novikov, Kornelius Nielsch, Stoichiometry of nickel oxide films prepared by ALD. *Chem. Vap. Deposition* **17**, 177–180 (2011)

19. T.S. Yang, W. Cho, M. Kim, K.-S. An, T.-M. Chung, C.G. Kim, Y. Kim, Atomic layer deposition of nickel oxide films using Ni (dmamp) 2 and water. *J. Vac. Sci. Technol., A* **23**, 1238 (2005)
20. M. Predanocy, I. Hotovy, M. Čaplovičová, Structural, optical and electrical properties of sputtered NiO thin films for gas detection. *Appl. Surf. Sci.* **395**, 208–213 (2016)
21. Q. Dong, S. Yin, C. Guo, X. Wu, N. Kumada, T. Takei, A. Miura, Y. Yonesaki, T. Sato, Single-crystalline porous NiO nanosheets prepared from  $\beta$ -Ni(OH)<sub>2</sub> nanosheets: magnetic property and photocatalytic activity. *Appl. Catal. B* **147**, 741–747 (2014)
22. T.T. Dang, M. Tonezzer, Polycrystalline NiO nanowires: scalable growth and ethanol sensing. *Procedia. Eng.* **120**, 427–434 (2015)
23. J.M. Choi, J.H. Byun, S.S. Kim, Influence of grain size on gas-sensing properties of chemiresistive p-type NiO nanofibers. *Sens. Actuators B* **227**, 149–156 (2016)
24. Y. Lu, Y.H. Ma, S.Y. Ma, W.X. Jin, S.H. Yan, X.L. Xu, X.H. Jiang, T.T. Wang, H.M. Yang, H. Chen, Z. Qiang, Synthesis of cactus-like NiO nanostructure and their gas-sensing properties. *Mater. Lett.* **164**, 48–51 (2016)
25. N.G. Cho, I.S. Hwang, H.G. Kim, J.H. Lee, I.D. Kim, Gas sensing properties of p-type hollow NiO hemispheres prepared by polymeric colloidal templating method. *Sens. Actuators B* **155**, 366–371 (2011)
26. P. Wu, J.H. Sun, Y.Y. Huang, G.F. Gu, D.G. Tong, Solution plasma synthesized nickel oxide nanoflowers: an effective NO<sub>2</sub> sensor. *Mater. Lett.* **82**, 191–194 (2012)
27. B. Liu, H. Yang, H. Zhao, L. An, L. Zhang, R. Shi, L. Wang, L. Bao, Y. Chen, Synthesis and enhanced gas-sensing properties of ultralong NiO nanowires assembled with NiO nanocrystals. *Sens. Actuators, B* **156**, 251–262 (2011)
28. X.H. Xia, J.P. Tu, J. Zhang, X.L. Wang, W.K. Zhang, H. Huang, Electrochromic properties of porous NiO thin films prepared by a chemical bath deposition. *Sol. Energy Mater. Sol. Cells* **92**, 628–633 (2008)
29. Romain Brisse, Rita Faddoul, Tiphaine Bourgeteau, Denis Tondelier, Jocelyne Leroy, Stéphane Campidelli, Thomas Berthelot, Bernard Geffroy, Bruno Jousselme, Ink-jet printing NiO-based p-type dye sensitized solar cells. *ACS Appl. Mater. Interfaces.* **9**, 2369–2377 (2016)
30. Hai-peng Cui, Jian-chang Li, Hai-lin Yuan, Bending effect on the resistive switching behavior of a NiO/TiO<sub>2</sub> p–n heterojunction. *RSC Adv.* **8**, 19861–19867 (2018)
31. M.A. Nasser, F. Kamali, B. Zakerinasab, Catalytic activity of reusable nickel oxide nanoparticles in the synthesis of spirooxindoles. *RSC Adv.* **5**, 26517–26520 (2015)
32. G. Evmenenko, T.T. Fister, F. Castro, X. Chen, B. Lee, D.B. Buchholz, V. Dravid, P. Fenter, M.J. Bedzyk, Structural analysis of initial lithiation of NiO thin film electrodes. *Phys. Chem. Chem. Phys.* **21**, 8897–8905 (2019)
33. C. Hu, K. Chu, Y. Zhao, W.Y. Teoh, Efficient photoelectrochemical water splitting over anodized p-Type NiO porous films. *ACS Appl. Mater. Interfaces.* **6**, 18558–18568 (2014)
34. P. Subalakshmi, A. Sivashanmugam, Fuel aided synthesis of NiO flakes for electrochemical energy storage application. *J. Alloys Compd.* **662**, 200–207 (2016)
35. Yuko Ichiyana, Naoto Wakabayashi, Junichiro Yamazaki, Saori Yamada, Yoshihide Kimishima, Eriko Komatsu, Hiroyuki Tajim, Magnetic properties of NiO nanoparticles. *Phys. B* **329**, 862–863 (2003)
36. Manisha Tyagi, Monika Tomar, Vinay Gupta, Optical properties of NiO thin films: a potential material for optoelectronic devices. *Adv. Mater. Res.* **488–489**, 103–108 (2012)
37. K. Uchida, K.-I. Yoshida, D. Zhang, A. Koizumi, S. Nozaki, High-quality single crystalline NiO with twin phases grown on sapphire substrate by metalorganic vapor phase epitaxy. *AIP Adv.* **2**, 042154 (2012)
38. S. Jana, G. Mondal, B.C. Mitra, P. Bera, B. Chakraborty, A. Mondal, A. Ghosh, Facile synthesis of nickel oxide thin films from PVP encapsulated nickel sulfide thin films: an efficient material for electrochemical sensing of glucose, hydrogen peroxide and photodegradation of dye. *New J. Chem.* **41**, 14985–14994 (2017)
39. S.T. Navale, V.V. Mali, S.A. Pawar, R.S. Mane, M. Naushad, F.J. Stadler, V.B. Patil, Electrochemical Supercapacitor Development Based on Electrodeposited Nickel Oxide Film. *RSC Adv.* **5**, 51961–51965 (2015)
40. Shuqin Shang, Keyan Xue, Dairong Chen, Xiuling Jiao, Preparation and characterization of rose-like NiO nanostructures. *CrystEngComm* **13**, 5094 (2011)
41. D. Fironi, *Surface effects in magnetic nanoparticles* (Springer, New York, 2005), p. 550
42. P. Ravikumar, B. Kisan, A. Perumal, Enhanced room temperature ferromagnetism in antiferromagnetic NiO nanoparticles. *AIP Adv.* **5**, 087116 (2015)
43. Y. Huang, X. Huang, J. Lian, D. Xu, L. Wang, X. Zhang, Self-assembly of ultrathin porous NiO nanosheets/graphene hierarchical structure for high-capacity and high-rate lithium storage. *J. Mater. Chem.* **22**, 2844–2847 (2012)
44. Ranjit S. Kate, Suraj C. Bulakhe, Ramesh J. Deokate, Effect of substrate temperature on properties of nickel oxide (NiO) thin films by spray pyrolysis. *J. Electron. Mater.* **48**, 3220–3228 (2019)
45. A.M. Bakry, S.A. Mahmoud, Effect of substrate temperature on the optical dispersion of sprayed nickel oxide thin films, saudi international electronics. *Commun. Photon. Conf. (SIECPC)*. (2011). <https://doi.org/10.1109/SIECPC.2011.5876956>
46. G. Ojeda-Barrero, A.I. Oliva-Avilés, A.I. Oliva, R.D. Maldonado, M. Acosta, G.M. Alonzo-Medina, Effect of the substrate temperature on the physical properties of sprayed-CdS films by using an automatized perfume atomizer. *Mater. Sci. Semicond. Process.* **79**, 76 (2018)
47. M. Ravikumar, R. Chandramohan, K.D. Arun Kumar, S. Valanarasu, A. Kathalingam, V. Ganesh, M. Shkir, S. AlFaify, Effect of Gd<sup>3+</sup> doping on key structural, morphological, optical, and electrical properties of CdO thin films fabricated by spray pyrolysis using perfume atomizer. *J. Sol-Gel. Sci. Technol.* **85**, 31 (2017)
48. M. Anitha, L. Amalraj, N. Anitha, Influence of precursor concentration on physical properties of CdO thin films prepared by spray pyrolysis technique using nebulizer. *Appl. Phys. A* **123**, 764 (2017)
49. M. Mhadhbi, M. Khitouni, L. Escoda, J.J. Sunol, M. Dammakl, Characterization of mechanically alloyed nanocrystalline Fe(Al) crystallite size and dislocation density. *J. Nanomater.* <https://doi.org/10.1155/2010/712407> (2010)
50. V. Sivaranjani, P. Philominathan, Influence of substrate temperature on physical properties of nanostructured Ti doped In<sub>2</sub>O<sub>3</sub> thin films by a simplified perfume atomizer technique. *Int. J. Thin. Film. Sci. Tech.* **4**, 219–225 (2015)
51. U.M. Patil, R.R. Salunkhe, K.V. Gurav, C.D. Lokhande, Chemically deposited nanocrystalline NiO thin films for supercapacitor application. *Appl. Surf. Sci.* **255**, 2603–2607 (2008)
52. S. Dey, C. Ghosh, S. Bhattacharjee, M. Ghosh Chaudhuri, R.S. Bose, S. Halder, Synthesis of pure nickel(III) oxide nanoparticles at room temperature for Cr(VI) ion removal. *RSC Adv.* **5**, 54717–54726 (2015)
53. M. Najafi, H. Eshghi, The effect of Cu-doping on physical properties of nanostructured NiO thin films prepared by spray pyrolysis technique. *Sci. Iran. Trans. F Nanotechnol.* **22**, 1317–1321 (2015)
54. T. Sivaraman, V.S. Nagarethnam, A.R. Balu, CdS thin films fabricated by a simplified spray technique from different substrate temperatures—structural, morphological, optical and electrical analysis. *Res. J. Mater. Sci.* **2**, 6–15 (2014)

55. M. Krunk, J. Soon, T. Unt, A. Mere, V. Mikli, Deposition of p-type NiO films by chemical spray pyrolysis. *Vacuum* **107**, 242–246 (2014)
56. J.D. Hwang, T.H. Ho, Effects of oxygen content on the structural, optical, and electrical properties of NiO films fabricated by radio-frequency magnetron sputtering. *Mater. Sci. Semicond. Process.* **71**, 396–400 (2017)
57. Sikai Zhao, Yanbai Shen, Pengfei Zhou, Jin Zhang, Wei Zhang, Xiangxiang Chen, Dezhou Wei, Ping Fang, Yansong Shen, Highly selective NO<sub>2</sub> sensor based on p-type nanocrystalline NiO thin films prepared by sol–gel dip coating. *Ceram. Int.* **44**, 753–759 (2018)
58. D. Desai, S.-K. Min, K.-D. Jung, O.-S. Joo, Spray pyrolytic synthesis of large area NiO<sub>x</sub> thin films from aqueous nickel acetate solutions. *Appl. Surf. Sci.* **253**, 1781–1786 (2006)
59. O.K. Ukoba, F.L. Inambao, A.C. Eloka-Eboka, Experimental optimization of nanostructured nickel oxide deposited by spray pyrolysis for solar cells application. *Int. J. Appl. Eng. Res.* **13**, 3165–3173 (2018)
60. M.L. Grilli, S. Aydogan, M. Yilmaz, A study on non-stoichiometric p-NiO<sub>x</sub>/n-Si heterojunction diode fabricated by RF sputtering Determination of diode parameters. *Superlattices Microstruct.* **100**, 924–933 (2016)
61. Bussarin Ksapabutr, Pathompong Nimnuan, Manop Panapoy, Dense and uniform NiO thin films fabricated by one-step electrostatic spray deposition. *Mater. Lett.* **153**, 24–28 (2015)
62. Mengying Wang, Yohann Thimont, Lionel Presmanes, Xungang Diao, Antoine Barnabé, The effect of the oxygen ratio control of DC reactive magnetron sputtering on as-deposited non stoichiometric NiO thin films. *Appl. Surf. Sci.* **419**, 795–801 (2017)
63. R. Newman, R.M. Chrenko, Optical properties of nickel oxide. *Phys. Rev.* **114**, 1507–1513 (1959)
64. Adèle Renaud, Benoit Chavillon, Laurent Cario, Loïc Le Pleux, Nadine Szuwarski, Yann Pellegrin, Errol Blart, Eric Gautron, Fabrice Odobel, Stephane Jobic, Origin of the black color of NiO used as photocathode in p–type dye-sensitized solar cells. *J. Phys. Chem. C* **117**, 22478–22483 (2013)
65. T. Taşköprü, E. Turan, M. Zor, Characterization of NiO films deposited by homemade spin coater. *Int. J. Hydrogen Energy* **41**, 6965–6971 (2015)
66. Fatemeh Hajakbari, Characterization of nanocrystalline nickel oxide thin films prepared at different thermal oxidation temperatures. *J. Nanostruct. Chem.* **10**, 97–103 (2020)
67. Abhijit A. Yadav, U.J. Chavan, Influence of substrate temperature on electrochemical supercapacitive performance of spray deposited nickel oxide thin films. *J. Electroanal. Chem.* **782**, 36–42 (2016)
68. V. Gupta, A. Mansingh, Influence of post deposition annealing on the structural and optical properties of sputtered zinc oxide film. *J. Appl. Phys.* **80**, 1063–1073 (1996)
69. K. Nadarajah, C. Yern Chee, C. Yong Tan, Influence of annealing on properties of spray deposited ZnO thin films. *J. Nanomater.* **16**, 1–8 (2013)
70. Rafia Barir, Boubaker Benhaoua, Soufiane Benhamida, Achour Rahal, Toufik Sahraoui, Rachid Gheriani, Effect of precursor concentration on structural optical and electrical properties of NiO thin films prepared by spray pyrolysis. *J. Nanomater.* <https://doi.org/10.1155/2017/5204639> (2017)
71. M. Jlassi, I. Sta, M. Hajji, H. Ezzaouia, Optical and electrical properties of nickel oxide thin films synthesized by sol–gel spin coating. *Mater. Sci. Semicond. Process.* **21**, 7–13 (2014)
72. H.K. Li, T.P. Chen, S.G. Hu, X.D. Li, Y. Liu, P.S. Lee, X.P. Wang, H.Y. Li, G.Q. Lo, Highly spectrum-selective ultraviolet photodetector based on p-NiO/n-IGZO thin film heterojunction structure. *Opt. Express* **23**, 27683–27689 (2015)
73. S. Manimena, G. Umadevi, M. Manickam, Effect of copper concentration on the physical properties of copper doped NiO thin films deposited by Spray pyrolysis. *Mater. Chem. Phys.* **191**, 181–187 (2017)
74. B.J. Rani, B. Saravanakumar, G. Ravi, V. Ganesh, A. Sakunthala, R. Yuvakkumar, Structural, Optical and Magnetic properties of NiO nanopowders. *J. Nanosci. Nanotechnol.* **18**, 4658–4666 (2018)
75. G.N. Narayanan, K. Annamalai, Role of hexamethylenetetramine concentration on structural, morphological, optical and electrical properties of hydrothermally grown zinc oxide nanorods. *J. Mater. Sci. Mater. Electron.* **27**, 12209–12215 (2016)
76. K. Anandan, V. Rajendran, Structural, optical and magnetic properties of well- dispersed NiO nanoparticles synthesized by CTAB assisted solvothermal process. *Nanosci. Nanotechnol. Int. J.* **2**, 24–29 (2012)
77. D. Adler, J. Feinleib, Electrical and optical properties of narrow-band materials. *Phys. Rev. B.* **2**, 3112–3134 (1970)
78. L. De Los Santos Valladares, A. Ionescu, S. Holmes, C.H.W. Barnes, Characterization of Ni thin films following thermal oxidation in air. *J. Vac. Sci. Technol. B* **32**, 051808-7 (2014)
79. V. Gowthami, P. Perumal, R. Sivakumar, C. Sanjeeviraja, Structural and optical studies on nickel oxide thin film prepared by nebulizer spray technique. *Phys. B* **452**, 1–6 (2014)
80. B. Kisan, P. Ravikumar, A. Das, A. Srinivasan, A. Perumal, Structural, vibrational, optical and magnetic properties of NiO nanoparticles. *Sci. Lett. J.* **4**, 160 (2015)
81. N. Mironova-Ulmane, A. Kuzmin, I. Sildos, L. Puust, J. Grabis, Magnon and Phonon Excitations in Nanosized NiO. *Latv. J. Phys. Tech. Sci.* **56**, 61–72 (2019)
82. K. Srinivas, S. Manjunath Rao, P. Venugopal Reddy, Structural, electronic and magnetic properties of Sn<sub>0.95</sub>Ni<sub>0.05</sub>O<sub>2</sub> nanorods. *Nanoscale.* **3**, 642–653 (2011)
83. S.S. Nkosi, B. Yalisi, D.E. Motaung, J. Keartland, E. Sideras-Haddad, A. Forbes, B.W. Mwakikunga, Antiferromagnetic–paramagnetic state transition of NiO synthesized by pulsed laser deposition. *Appl. Surf. Sci.* **265**, 860–864 (2013)
84. H.T. Rahal, R. Awad, A.M. Abdel-Gaber, D. El-Said Bakeer, Synthesis, characterization, and magnetic properties of pure and EDTA-capped NiO nanosized particles. *J. Nanomater.* **2017**, 1–9 (2017)
85. Jian Zhang, Dawen Zeng, Qiang Zhu, Wu Jinjin, Qingwu Huang, Changsheng Xie, Effect of nickel vacancies on the room-temperature NO<sub>2</sub> sensing properties of mesoporous NiO nanosheets. *J. Phys. Chem. C* **120**, 3936–3945 (2016)
86. K. Sudalai Muthu, P. Perumal, Synthesis and characterization of NiO Nanoparticles using egg white method. *J. Mater. Sci. Mater. Electron.* **28**, 9612–9617 (2017)
87. N. Pathak, S.K. Gupta, C.L. Prajapat, S.K. Sharma, P.S. Ghosh, B. Kanrar, P.K. Pujari, R.M. Kadam, Defect induced ferromagnetism in MgO and its exceptional enhancement upon thermal annealing: a case of transformation of various defect states. *Phys. Chem. Chem. Phys.* **19**, 11975–11989 (2017)

**Publisher's Note** Springer Nature remains neutral with regard to jurisdictional claims in published maps and institutional affiliations.